Accepted Manuscript

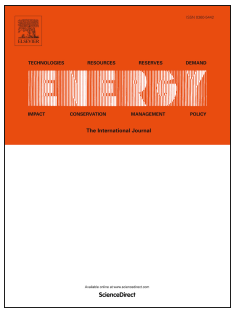

Development and experimental investigation of a 500-W class ultra-micro gas turbine power generator

JeongMin Seo, Hyung-Soo Lim, Jun Young Park, Moo Ryong Park, Bum Seog Choi

PII: S0360-5442(17)30186-X

DOI: 10.1016/j.energy.2017.02.012

Reference: EGY 10305

To appear in: *Energy*

Received Date: 19 August 2015

Revised Date: 1 February 2017

Accepted Date: 2 February 2017

Please cite this article as: Seo J, Lim H-S, Park JY, Park MR, Choi BS, Development and experimental investigation of a 500-W class ultra-micro gas turbine power generator, *Energy* (2017), doi: 10.1016/j.energy.2017.02.012.

Title:

Development and experimental investigation of a 500-W class ultra-micro gas turbine power generator

Author names and affiliations:

JeongMin Seo, Hyung-Soo Lim, Jun Young Park, Moo Ryong Park, and Bum Seog Choi

Department of Extreme Energy Systems, Korea Institute of Machinery & Materials

171 Jang-dong, Yuseong-gu, Daejeon, Republic of Korea, 34103

JeongMin Seo: jmseo@kimm.re.kr

Hyung-Soo Lim: limbo999@kimm.re.kr

Jun Young Park: jypark@kimm.re.kr

Moo Ryong Park: mrpark@kimm.re.kr

Bum Seog Choi: bschoi@kimm.re.kr

Corresponding author:

Dr. JeongMin Seo

Department of Extreme Energy Systems, Korea Institute of Machinery & Materials,

171 Jang-dong, Yuseong-gu, Daejeon, Republic of Korea, 34103

Tel. +82-42-868-7541

E-mail: jmseo@kimm.re.kr

Abstract:

We experimentally investigate the feasibility of a 500-W class ultra-micro gas turbine power generator. System specifications include a design rotational speed of 400,000 rpm, a compressor ratio of 3:1, and a turbine inlet temperature of 1200K. In a previous study, we used an integrated test rig to examine the feasibility of start-up and self-sustaining capabilities. Here, we describe our development and testing of a new integrated test rig to measure the performance of electric-power generation during self-sustaining and boosting operations. We controlled a motor-generator using an electric controller in fixed speed mode and guided the rotational speed according to the start-up sequence. We employed a radial-thrust integral metal-mesh bumper air foil bearing with which we obtained the design rotational speed of 400,000 rpm in a standalone motoring test. In the combustor, we used liquefied petroleum gas as the main fuel and kerosene as the ignition fuel and partially as the main fuel during the boost operation. The integrated test rig achieved electric power generation of 30 W at 200,000 rpm, 50% of the design rotational speed.

Keywords:

Ultra-micro gas turbine; electric power generation; experimental investigation; self-sustaining and boosting test

Nomenclature, Abbreviations and Acronyms

Nomenclature

M	mass flow rate
P	power
Pr	pressure ratio
Pr_{TS}	total-to-static pressure ratio
Q	volume flow rate
s	entropy
t	time
T	temperature
η_{th}	thermal efficiency

Abbreviations and Acronyms

AFR	Air Fuel Ratio
AIST	National Institute of Advanced Industrial Science and Technology
CFD	Computational Fluid Dynamics
CNC	Computer Numerical Control
IHI	Ishikawajima-Harima Heavy Industries Co., Ltd.
IHPC	Institute of High Performance Computing
KIMM	Korea Institute of Machinery & Materials
LPG	Liquefied Petroleum Gas
MEMS	Micro-Electro-Mechanical Systems
MFC	Mass Flow Controller
MIT	Massachusetts Institute of Technology
MMBFB	Metal-Mesh Bumper-Foil Bearing
SIMTech	Singapore Institute of Manufacturing Technology

TIT	Turbine Inlet Temperature
UMGT	Ultra-Micro Gas Turbine

1. Introduction

As the usage of mobile devices has increased over the past few decades, there have been significant developments in technologies related to mobile devices. For example, in the case of notebooks, disk capacity has increased by a factor of several thousand, and CPU speeds and available RAM capacity have also increased by factors of several hundred. However, the energy densities of batteries have increased by only a relatively small amount during this period. This is why power sources are bottlenecks in mobile technologies. Secondary batteries, such as lithium ion, nickel-cadmium, and nickel-metal hydride, are the most widely used power sources in mobile devices, which include smart phones, digital cameras, and notebooks. Recently, there has been an increasing demand for mobile devices with moving parts, such as unmanned ground vehicles, unmanned aerial vehicles, and humanoid robots, which require power systems with higher power and energy densities. Secondary batteries are not sufficient to provide electric power to these devices because of their low energy densities. Fuel cells, while considered to be a good solution with high energy density, enabling long operation times, have a poor power density, which restricts their widespread implementation as mobile power sources. Power sources with both high power densities and high energy densities include internal combustion engines. Further, micro gas turbines are more suitable than other types of internal combustion engines because of their higher power density, continuous combustion, and continuous rotation [1].

Several research groups have been involved in the development of micro gas turbines from two perspectives. One is the Micro-Electro-Mechanical Systems (MEMS)-based micro gas turbine engine proposed by a group at Massachusetts Institute of Technology (MIT) [2-4]. A nickel (US coin)-sized gas turbine with a mass less than 1 g has been developed using silicon wafer fabrication technology. Large volumes of MEMS-based turbines designed in a 2D shape can be made from silicon wafers at low cost and with high accuracy. Similar studies and developments have been conducted by the groups at Singapore Institute of Manufacturing Technology (SIMTech) in Singapore, Institute of High Performance Computing (IHPC) in Singapore, National Institute of Advanced Industrial Science and

Technology (AIST) in Japan [5,6], Tohoku University in Japan [7,8], Michigan State University [9,10], and the University of Tokyo in Japan [11]. In spite of the extensive research on MEMS-based micro gas turbines, there remain several critical problems to be overcome. Silicon wafer fabrication technology restricts the choice of materials and the design flexibility. Further, heat loss from the large area-to-volume ratio decreases the gas turbine performance. The instability of combustion in a small combustor chamber leads to decreased chamber-wall cooling and burning in the recirculation channel, which can damage the device because of the high wall temperature. These critical problems related to MEMS-based micro gas turbines have led to the development of machining-based 3D design micro gas turbines that are made using various high-precision machining techniques such as micro molding, micro electrical discharge machining, and 5-axis Computer Numerical Control (CNC) micro milling. Machining-based 3D design micro gas turbines have been proposed by downsizing traditional gas turbines. Related studies have been conducted by groups at the Tohoku University, the Tohoku-Gakuin University, the University of Tokyo, Ishikawajima-Harima Heavy Industries Co., Ltd. (IHI) in Japan [1,12-14], Katholieke Universiteit Leuven in Belgium [15] and Stanford University [16,17]. Machining-based 3D design micro gas turbines enable a greater choice of materials, such as steel alloys, nickel alloys, and ceramics, and there is also design flexibility referable to the well-established design of conventional gas turbines. Finally, the world's smallest class gas turbine engine with a Brayton cycle was demonstrated in 2007 [14]. However, the demonstration was not sufficient for mobile power generation because it employed externally pressurized gas bearings that required an external pressure source, and it had no electric power output because it used a dummy electromagnetic generator.

A micro gas turbine with a machining-based 3D design has been under development since 2008 by our research group at Korea Institute of Machinery & Materials (KIMM) [18-22]. The goal of the project is to prove the feasibility of 500-W of generated electric power using an Ultra-Micro Gas Turbine (UMGT) with a 1 l volume for mobility. Additionally, we have developed integrated test equipment to analyze the performance of the system. With the first set of integrated test equipment, we

demonstrated the start-up and self-sustaining performance of the UMGT. However, electric power production could not be measured using the first integrated test equipment. In this study, we developed and tested an improved model of integrated test equipment for electric power generation.

2. Specifications

To develop a 500-W UMGT power generator with a 1 l volume, we obtained design specifications such as system size, efficiency, power, turbine inlet temperature, rotational speed, and compression pressure ratio by performing cycle analysis using GasTurb 11 [23]. For the thermal cycle analysis, we applied a single spool with a recuperator model in the program. Fig. 1 shows the configuration of the cycle and the thermodynamic station designation in GasTurb 11. We selected a Turbine Inlet Temperature (TIT) of 1200 K, accounting for the melting temperature of commercial alloys and the margin of safety for creep resistance, non-uniformity of the combustion flame and centrifugal force by the blade rotation. We used a pressure ratio of 3 based on general centrifugal compressor performance. Assumptions of the efficiencies of components were made through a literature survey considering the small scale of the system [24-26], and they were updated from the results of performing computations and experiments for each component. Table 1 presents the preconditions for the cycle analysis. Fig. 2 illustrates the relationships of shaft power and thermal efficiency to changes in pressure ratio and TIT. Based on the requirements of system power and the thermal efficiency, we selected the design point of the cycle; Fig. 3 presents the T-s diagram of the cycle. The results of the cycle analysis are summarized in Table 2.

We designed the system layout considering the aerodynamics, which includes the flow path and heat loss, and the rotor dynamics, which involves the bearing and shaft, heat expansion, and assembly. The schematic cross section of the 500-W UMGT power generator is shown in Fig. 4; it is composed of a centrifugal compressor, a radial turbine, an annular combustor, six recuperators, a motor-generator and auxiliaries. Because the system has a high rotational speed, the stability of the rotor dynamics is very important. To increase the rotor dynamic stability, the rotor length was shortened, and the generator

was directly connected to the compressor and turbine. The efficiency of the generator decreases as its temperature increases. Heat is not only transferred from the combustor through the rotor shaft, but is also generated during operation. This layout helps to cool the generator using inlet air.

We selected a centrifugal-type compressor and a one-stage radial turbine for the UMGT because of its small mass-flow rate and relatively large pressure ratio. We applied a vaneless diffuser for the compressor because of its wide operating range. We conducted non-dimensional parameter study for design selection of the compressor and the turbine. We chose a rotational speed of 400,000 rpm to obtain specific speeds for the compressor of 0.65 and for the turbine of 0.70 using the characteristics of the thermodynamic cycle and the mass flow rate. In the design procedure, iterative processes from 1D design to 3D Computational Fluid Dynamics (CFD) of compressors and turbines were required to conform that the designed geometries met the design conditions. We used commercial 1D design programs, ConceptsNREC COMPAL [27] for centrifugal compressors and ConceptsNREC RITAL [28] for radial turbines. The geometries obtained from 1D design were evaluated using a commercial 3D Computational Fluid Dynamics (CFD) program, ANSYS CFX [29]. The design parameters of the compressor are listed in Table 3. We performed the structural simulations of the turbine to analyze the material stress and strain caused by high temperatures and high rotational speeds. The design parameters of the turbine are shown in Table 4.

Although a multiple-can-type combustor has an advantage in terms of its flame stability, we selected an annular-type combustor to reduce the overall system size. This combustor consists of 12 fuel nozzles, one heater for the ignition, an inner liner, an outer liner, and an inner/outer case. There are two fuel choices, liquid fuel and gas fuel. Systems that use gas fuel require a small fuel-injection compressor with a high-compression pressure ratio over 3 bar, which is the pressure in the combustor. They also need large and heavy fuel storage tanks. These attenuate the mobility and the compactness of systems. Therefore, we designed the UMGT power generator to use liquid fuel (kerosene) as the main fuel and the ignition fuel. However, we used gas fuel, Liquefied Petroleum Gas (LPG), as the main fuel in this study. The test rig as well as the driving sequence logic has not been stabilized at this

writing. The test rig for this study was designed for gas fuel, which has advantages in the stability of its combustion flame. To improve the efficiency of the system, we also employed recuperators. Based on cycle analysis, recuperators increase the system efficiency by approximately 4%. The recuperator system that was employed is composed of six recuperators positioned symmetrically outside of the combustor. Each recuperator consists of 11 stacked plates.

3. Experimental Setup

3.1 First integrated test rig

We developed the first integrated test rig and presented the test results in a previous study [22]. We developed it to examine the performance of the UMGT power generator, as shown in Fig. 5. The test rig consisted of a compressor, a turbine and a combustor, as summarized in Table 5. The compressor and the turbine manufactured by 5-axis CNC micro-milling were connected in the back-to-back arrangement with a shaft. Instead of electric spark igniters, we used a commercial graphite hot-bulb igniter to reduce the system-weight. Recuperators were not applied. We designed a 500-W UMTG to use kerosene for the igniter fuel and the main fuel, but we used LPG as the main fuel in the test rig because of the flame instability problem.

We demonstrated start-up and self-sustaining performance. However, the first integrated test rig had several problems. It used an air-impingement starter, so it was difficult to realize operation following the starting sequence logic. The radial-thrust integral static-air bearing applied in the test rig had an operating limit of 250,000 rpm, which was 62.5% of the design speed. Because there was no generator, generated power could not be measured using this test rig. In the present study, we developed a new integrated test rig to address these problems.

3.2 Second integrated test rig

Fig. 7 shows the second integrated test rig designed to address the problems above. It consists of a compressor, a turbine, a combustor and a motor-generator. The motor-generator was placed in front of

the compressor inlet, as shown in Fig. 8(a). The motor-generator could be regulated by an electric controller with both a fixed-speed mode and a fixed-torque mode. In the fixed-speed mode, the motor was automatically switched to a generator by the controller when the torque of the turbine was greater than that of motoring at fixed speed. We used the same designs of the compressor and turbine as those of the first integrated test rig. To enhance the rotor dynamic stability, the compressor and turbine were made from a single piece of Inconel 718. The tip gaps of the compressor and the turbine were designed as 0.1 mm. During several tests, some failures were caused by the turbine blade tip touching the shroud due to thermal expansion of the materials by hot gas from the combustor and by the axial movement of the axis because of high axial thrust force. To prevent damage, we modified the tip gap of the turbine to 0.2 mm. In the future, we will study and test the relationship between performance and various turbine tip gaps. Using the shrink fit method, we connected the assembly of the compressor and turbine to the sleeve, which contains a neodymium-iron-boron (NdFeB) permanent magnet. The rotor shaft was designed with a diameter of 11.6 mm, as shown in Fig. 8(b). Between the compressor and the turbine, we applied the radial-thrust integral Metal-Mesh Bumper-Foil Bearing (MMBFB) shown in Fig. 8(c). In a standalone motoring test for the bearing, the rotational speed reached the design speed of 400,000 rpm. We improved the annular-type combustor used in the first integrated test rig. We optimized the tilt angle and length of the flame holder, and we modified the diameter and type of air-admission hole to increase the flame stability by enhancing the air flow and swirl effect. We performed a standalone performance test for the combustor to determine the possible ignition conditions. Depending on the rotational speed, the air-mass flow rate and total pressure ratio can generally be determined, and we could obtain the correct fuel-mass flow rate.

We established the test bench as shown in Fig. 9. We measured the ambient temperature and the temperatures at the compressor outlet, the turbine inlet, and the exhaust, as well as the ambient pressure and pressures at the inlet nozzle and the compressor outlet. We installed the nozzle flowmeter in front of the motor-generator, and calculated the mass flow rate of air using the ambient pressure, nozzle pressure, and ambient temperature. The measurement uncertainties of temperature and pressure

were ±0.2% and ±0.5% of design points, respectively, at a 95% confidence level. We measured the rotational speed using an optical speed sensor, and monitored it using the controller of the motor-generator. The mass flow rate of the igniter fuel and the volume flow rate of the main fuel were also controlled and monitored.

4. Results

The results of the electric power generation test are shown in Fig. 10(a)-(f). The self-sustaining test results are the blue dotted lines. The rotational speed of the motor-generator was regulated using the controller. To ignite the combustor, the speed was accelerated to the ignition target speed of 120,000 rpm, which is 30% of the design speed for the self-sustaining and boosting tests. The graphite hot bulb igniter started warming up approximately 10 sec before the start of igniter-fuel injection. We then injected the igniter fuel with a mass flow rate of 1.0 g/min, as shown in Fig. 10(a). At this point, the measurement time started at 0 sec. After 31 sec, we started to inject main fuel at the volume-flow rate of 1.7 l/min, as shown in Fig. 10(b). After 9 sec of main fuel injection, we turned off the igniter fuel. At the fixed rotational speed of 150,000 rpm, we increased the main fuel to 3.4 l/min at 190 sec continuing until 600 sec. Fig. 10(c) shows the rotational speed. The speed was governed by the controller in fixed speed mode. The design speed for ignition was 120,000 rpm, and we held the speed until 94 sec. We then increased the speed to 150,000 rpm and retained it during the self-sustaining test. Fig. 10(d) presents the total-to-static pressure ratio. The behavior of the pressure ratio was generally proportional to the rotational speed. Between 115 sec and 190 sec, the volume-flow rate of main fuel increased, but the pressure ratio was rarely changed. As expected, the mass flow rate of air in Fig. 10(e) synchronized with the rotational speed. The mass flow rate was also influenced by other variables. For example, it slightly decreased with the increase of the main fuel at a fixed speed between 115 sec and 190 sec. The mass flow rate of air was approximately 4.6 g/sec in the self-sustaining condition. Fig. 10(f) represents the air-fuel ratio of the main fuel. It was approximately 44 in the self-sustaining condition. Fig. 10(g) expressed TIT, which should be carefully controlled along

with the rotational speed to manage the risk of system failure. We restricted TIT to be under 1200 K. When the igniter fuel was ignited, the turbine inlet temperature increased slightly from 0 sec to 31 sec. According to theory, the behavior of TIT was proportional to the volume-flow rate of main fuel. We selected the rotational speed, 150,000 rpm, and the mass flow rate of main fuel, 3.4 l/min, to keep TIT between 1100 K and 1200 K in the self-sustaining condition. Fig. 10(h) shows the power output. While only the igniter fuel was injected, the power output was approximately -70 W. The negative value signifies that there is an electric power-input to the motor; the positive value means that an electric power output is produced by the generator. As the speed increased from 120,000 rpm to 150,000 rpm from 94 sec to 110 sec, the power output decreased from -13 W to -35 W. As the volume-flow rate of the main fuel increased from 2.1 l/min to 3.4 l/min with the rotational speed, 150,000 rpm, the power output went from a negative value to a positive value. The test rig produced a stable electric power output of approximately 5 W for longer than 5 min. Self-sustaining operation with electric-power generation was therefore considered to be successful.

The results of the boost performance test are denoted with the red solid lines in Fig. 10. The starting sequence logic of the boost test was similar to that of the self-sustaining test. As shown in Fig. 10(a)-(c), the igniter fuel was injected with a mass flow rate of 1.5 g/min at a rotational speed of 120,000 rpm, and the main fuel was injected with a volume-flow rate of 2.7 l/min at a rotational speed of 150,000 rpm. After 15 sec later, we stopped the injection of the igniter fuel. From 60 sec to 141 sec, the volume-flow rate of the main fuel was increased from 2.7 l/min to 5.1 l/min, and the rotational speed was accelerated from 150,000 rpm to 180,000 rpm. The TIT then reached 1050 K, and the UMGT power generator started to produce electric power. Although the 500-W UMGT was designed to use liquid fuel, this integrated test rig was developed to use LPG gas fuel, which was injected into the system from a compressed fuel-storage tank. As the rotational speed increased, the pressure difference between the compressor outlet and the main fuel storage tank decreased, and the maximum of the volume-flow rate of main fuel therefore decreased. While the rotation speed was 180,000 rpm, the maximum of the volume-flow rate of the main fuel was 5.1 l/min. Therefore, we could not increase

the volume-flow rate of the main fuel after 141 sec. To conduct a boosting test, we decided to use the igniter fuel as an additional main fuel. The injection of the igniter fuel began at 200 sec, and the mass flow rate of the igniter fuel increased from 1.0 g/s to 4.8 g/s, which was the maximum value for this test rig. While we raised the mass flow rate of the igniter fuel, the turbine inlet temperature increased. To maintain the turbine inlet temperature below the design turbine inlet temperature (1200 K), we enlarged the mass flow rate of air by accelerating the rotational speed from 180,000 rpm to 200,000 rpm. As in the self-sustaining test case, the total-to-static pressure ratio of the boosting test also appeared to be proportional to the rotational speed. The increased pressure ratio then reduced the volume flow rate of the main fuel. As shown in Fig. 10(h), the electric power generated increased from 5 W to approximately 30 W through the boosting test using the igniter-fuel injection. The boost operation with electric-power generation was therefore considered to be successful.

To examine the proper operation of the combustor under self-sustaining conditions, we used a chemical equilibrium analysis calculation. We selected the result at 420 sec in the self-sustaining test case, when the system was operated quasi-constantly. The temperature of the compressor outlet was 284.7 K, the pressure of the compressor outlet was 117.8 kPa, and the Air Fuel Ratio (AFR) of the main fuel was 42.57. The main fuel consisted of mole fractions of 96.9% of C_3H_8, 1.9% of C_4H_{10}, 1.0% of C_2H_6, and 0.2% of N_2. We conducted a chemical equilibrium calculation using STANJAN [30,31] in which we assumed that the gas was an ideal gas mixture and that the calculation conditions were a process at constant pressure and enthalpy. We had CO, CO_2, NO, H_2O as additional species present at equilibrium. The TIT in the experiment was 1148.8 K and the equilibrium temperature calculated by STANJAN was 1216.2 K. The temperature difference was 67.4 K, or 5.5% of the TIT. This is a reasonable value considering the heat loss through the wall.

To guarantee stable operation of the gas turbine system, the operating range of the compressor should be examined. The range of stable operation of the compressor is bounded by a surge and a choke. The surge, which is the left-hand limit in the low flow-rate region, causes reverse flow to occur; in extreme surge, the thrust bearings of the system can be damaged. The choke, which is the right-hand limit in

the high flow-rate region, is the thermodynamic limit of compressible flow. Fig. 11 shows a compressor performance map for the total-to-static pressure ratio obtained from the 1-D meanline analysis. The operations of the self-sustaining and boosting tests are shown in the performance map. The operations have sufficient margin from the surge line, which means that the compressor moves under stable conditions.

5. Conclusions

After a gas turbine at micro scale was proposed as a power generator for mobile devices, many researchers have been involved in developments of related technologies. Though many successful results in component level have been achieved, there have been few studies succeeded in producing electric power in the form of an intact gas turbine generator. The development of gas turbines at micro scale raises many new challenges [32]. Bearings and generators operable in the range between 300,000 rpm and 500,000 rpm should be completely developed. Tight tolerances cause difficulties on fabrication process and weakness for thermal expansion. The larger surface area to volume ratio promotes high heat transfer loss and high skin friction loss. Auxiliary components and accessories in starting, fuel, and control systems for gas turbines at micro scale should be also provided. The listed problems are critical issues in the miniaturization of gas turbine generators.

We have conducted a series of researches on gas turbines at micro scale. In this study, we developed the new integrated test rig to evaluate the performance of a 500-W UMGT power generator. The motor-starter realized operation following the starting sequence logic. We could obtain higher rotational speed using the radial-thrust integral metal-mesh bumper air foil bearing and measure the generated electric power using the motor-generator. The tests were conducted in three operating modes, namely start-up, self-sustaining, and boosting. The sequences of the operations were controlled by the rotational speed using the controller of a motor-generator with a fixed-speed mode. From the tests, we obtained the following results.

(1) In the self-sustaining operation, the test rig worked stably and produced 5 W of electric power at a rotational speed of 150,000 rpm with the main fuel being LPG.

(2) In the boost operation, the test rig reached 200,000 rpm and produced 30 W of electric power using both the main fuel, LPG, and the ignition fuel, kerosene.

(3) Through the chemical equilibrium calculation, we confirmed that the combustor worked normally.

(4) We conducted self-sustaining and boosting operations in the stable region maintaining a sufficient margin from the surge line.

Hence, we verified the feasibility of a 500-W UMGT power generator for electric-power generation and succeeded in obtaining generated power. In the future, we will attempt to modify the test equipment to enable it to use kerosene as the main fuel in order to supply enough fuel to the highly pressurized combustor.

Acknowledgments

This work was supported by the Next Generation Military Battery Research Center program of the Defence Acquisition Program Administration and Agency for Defence Development. Additional support was provided by the R&D Program at the Korea Institute of Machinery and Materials (KIMM), funded by the National Research Council of Science and Technology.

References

[1] Isomura K, Tanaka S, Togo S-I, Esashi M. Development of high-speed micro-gas bearings for three-dimensional micro-turbo machines. Journal of Micromechanics and Microengineering 2005;15:S222–7. doi:10.1088/0960-1317/15/9/S08.

[2] Epstein AH, Senturia SD, Anathasuresh G, Ayon A, Breuer K, Chen K-S, et al. Power MEMS and microengines. Proceedings of International Solid State Sensors and Actuators Conference (Transducers ’97) 1997;2. doi:10.1109/SENSOR.1997.635209.

[3] Epstein AH. Millimeter-scale, micro-electro-mechanical systems gas turbine engines. Journal of Engineering for Gas Turbines and Power 2004;126:205–26. doi:10.1115/1.1739245.

[4] Gong Y, Sirakov BT, Epstein AH, Tan CS. Aerothermodynamics of micro-turbomachinery. Proceedings of the ASME Turbo Expo 2004, vol. 6, MIT Gas Turbine Laboratory, Cambridge, MA 02139, United States: 2004, p. 95–102.

[5] Shan XC, Wang ZF, Jin YF, Wu M, Hua J, Wong CK, et al. Studies on a micro combustor for gas turbine engines. Journal of Micromechanics and Microengineering 2005;15:S215–21. doi:10.1088/0960-1317/15/9/S07.

[6] Shan XC, Zhang Q, Sun Y, Wang Z. Design, fabrication and characterization of an air-driven micro turbine device. Journal of Physics: Conference Series 2006;34:316–21. doi:10.1088/1742-6596/34/1/052.

[7] Kang P, Tanaka S, Esashi M. Demonstration of a MEMS-based turbocharger on a single rotor. Journal of Micromechanics and Microengineering 2005;15:1076–87. doi:10.1088/0960-1317/15/5/026.

[8] Nakajima A, Kang P, Honda N, Hikichi K, Esashi M, Tanaka S. Fabrication and high-speed characterization of SU-8 shrouded two-dimensional microimpellers. Journal of Micromechanics and Microengineering 2007;17:S230–6. doi:10.1088/0960-1317/17/9/S04.

[9] Iancu F, Piechna J, Muller N. Numerical solutions for ultra-micro wave rotors (UμWR). 35th AIAA Fluid Dynamics Conference and Exhibit, 2005.

[10] Iancu F, Zhu X, Tang Y, Alsam D, Muller N. Design and fabrication of microchannel test rig for ultra-micro wave rotors. Microsystem Technologies 2008;14:79–88. doi:10.1007/s00542-007-0402-5.

[11] Okamoto K, Nagashima T, Yamaguchi K. Design and Performance of a Micro Wave Rotor. 17th International Symposium on Airbreathing Engines, 2005.

[12] Tanaka S, Isomura K, Togo S-I, Esashi M. Turbo test rig with hydroinertia air bearings for a palmtop gas turbine. Journal of Micromechanics and Microengineering 2004;14:1449–54. doi:10.1088/0960-1317/14/11/003.

[13] Isomura K, Murayama M, Teramoto S, Hikichi K, Endo Y, Togo S, et al. Experimental verification of the feasibility of a 100 W class micro-scale gas turbine at an impeller diameter of 10 mm. Journal of Micromechanics and Microengineering 2006;16:S254–61. doi:10.1088/0960-1317/16/9/S13.

[14] Tanaka S, Hikichi K, Togo S, Murayama M, Hirose Y, Sakurai T, et al. World's smallest gas turbine establishing Brayton cycle. Technical Digest PowerMEMS2007, 2007, p. 359–62.

[15] Peirs J, Reynaerts D, Verplaetsen F. Development of an axial microturbine for a portable gas turbine generator. Journal of Micromechanics and Microengineering 2003;13:S190–5. doi:10.1088/0960-1317/13/4/328.

[16] Liu H-C, Kang S, Prinz FB, Stampfl J, Wien T. Fabrication of ceramic components for micro gas turbine engines. Ceramic Engineering and Science Proceedings, vol. 23, 2002, p. 43–50.

[17] Kang S, Johnston JP, Arima T, Matsunaga M, Tsuru H, Printz FB. Microscale radial-flow compressor impeller made of silicon nitride: Manufacturing and performance. Journal of Engineering for Gas Turbines and Power 2004;126:358–65. doi:10.1115/1.1739246.

[18] Han SJ, Seo JM, Park J-Y, Choi B-S, Do KH. Design and simulation of 500W ultra-micro gas turbine generator. Proceedings of the 10th Workshop on Micro and Nanotechnology for Power Generation and Energy Conversion Applications, 2010, p. 247–50.

[19] Seo J, Park J-Y, Choi B-S, Park M-R, Han SJ. Evaluation of 500W Ultra-micro Gas Turbine Compressor. PowerMEMS2011, 2011.

[20] Park CH, Choi SK, Hong DE, Yoon TG, Lee SH. Note: Radial-thrust combo metal mesh foil bearing for microturbomachinery. Review of Scientific Instruments 2013;84. doi:10.1063/1.4825037.

[21] Seo JM, Park JY, Choi BS. Start-up and self-sustain test of 500 W ultra-micro gas turbine generator. Journal of Physics: Conference Series 2013;476. doi:10.1088/1742-6596/476/1/012060.

[22] Seo JM, Lim HS, Choi BS, Park JY, Park MY. Development Status of Performance Evaluation Systems for 500W Ultra-Micro Gas Turbine Generator. Asian Congress on Gas Turbine 2014, 2014, p. AGGT2014–81.

[23] Kurzke J. GasTurb 11 User Manual.

[24] Hamilton SL. The Handbook of Microturbine Generators. Oklahoma: PennWell; 2003.

[25] Moore MJ, editor. Micro-turbine Generators. Suffolk, UK: Professional Engineering Publishing; 2002.

[26] Soares C. Gas Turbines: A Handbook of Air, Land, and Sea Applications. San Diego (CA): Elsevier; 2008.

[27] Concepts NREC. COMPAL Version 8.1.11.0. Concepts ETI Inc., 2013.

[28] Concepts NREC. RITAL Version 8.1.11.0. Concepts ETI Inc., 2013.

[29] ANSYS CFX. ANSYS CFX user's guide release 14.5. Canonsburg, ANSYS Inc., 2012.

[30] Reynolds WC. The Element-Potential Method for Chemical Equilibrium Analysis: Implementation in the Interactive Program STANJAN. Stanford University, 1986.

[31] Chemical Equilibrium Calculation. Available from: http://navier.engr.colostate.edu/~dandy/code/code-4/.

[32] Robinson A. Development and Testing of Hydrogen Fuelled Combustion Chambers for the Possible Use in an Ultra Micro Gas Turbine [Dissertation]. Bruxelles, Université libre de Bruxelles, Ecole polytechnique de Bruxelles, 2012.

List of Tables

Table 1. Design preconditions for cycle analysis.

Item	Unit	Value
Mass flow rate of air	kg/s	0.02
Compressor pressure ratio	-	3
TIT	K	1200
Compressor efficiency	%	70
Combustor efficiency	%	90
Turbine efficiency	%	70
Heat exchanger efficiency	%	75
Generator efficiency	%	80

Table 2. Design specifications.

Item	Unit	Value
Rotational speed	rpm	400,000
Fuel heating values	kJ/g	43.124
Mass flow rate of main fuel	g/s	0.1968
Turbine power	kW	4.13
Compressor power	kW	3.05

Shaft power	kW	1.08
Generator power	kW	0.86
Thermal efficiency	%	12.7

Table 3. Compressor design parameters.

Item	Unit	Value
Blade number	-	7+7
Impeller outlet radius	mm	11.4
Tip clearance	mm	0.1
Backswept angle	deg.	-43
Total to total compression pressure ratio	-	3.173
Total to total isentropic efficiency	%	78.96
Input power	W	2,868

Table 4. Turbine design parameters.

Item	Unit	Value
Number of nozzle blade	-	20
Nozzle blade inlet radius	mm	16.0
Nozzle exit blade angle	deg.	73.9
Number of rotor blade	-	8
Rotor blade inlet radius	mm	10.0
Rotor blade tip clearance	mm	0.1
Rotor exit blade angle	deg.	-43
Total to total pressure expansion ratio	-	2.52
Total to static pressure expansion ratio	-	2.98

Total to static isentropic efficiency	%	70
Output power	W	4,521

Table 5. Characteristics of components in the first integrated test rig.

Item	Figure	Characteristics
Compressor	Fig. 6(a)	pressure ratio 3.0; 7+7 blades; with vaneless diffuser
Turbine	Fig. 6(b)	20 nozzle blade; 8 rotor blade
Shaft	Fig. 6(c)	back to back arrangement of compressor and turbine
Bearing	Fig. 6(d)	radial and thrust all-in-one static air bearing; 15 bar static pressure by Nitrogen
Igniter	Fig. 6(e)	graphite hot-bulb igniter; kerosene as the igniter fuel
Combustor	Fig. 6(f)	annular-type; 12 nozzles; LPG as the main fuel
Starter	-	air impingement starter; manually operated

List of Figures

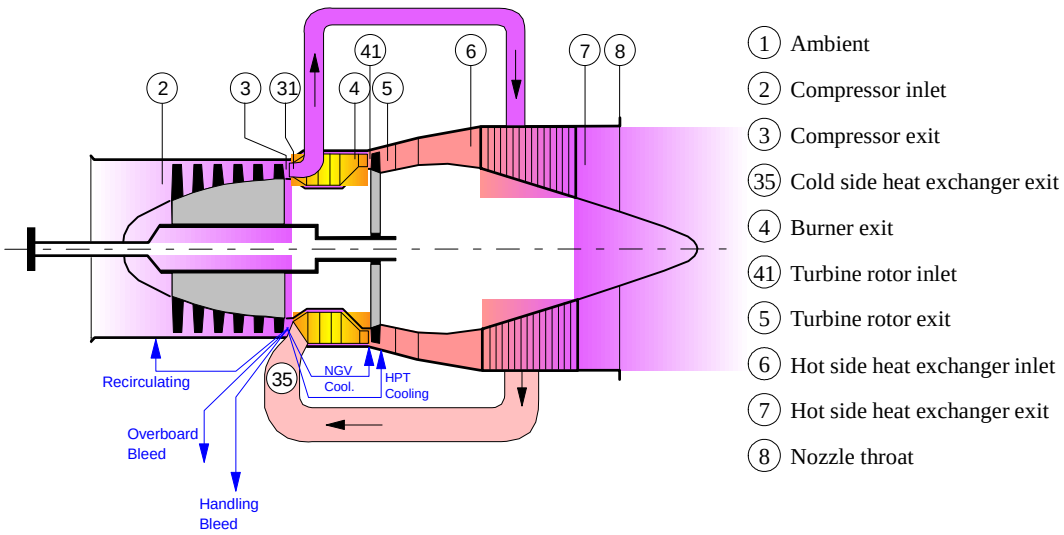

Fig. 1. Configuration of a single spool with a recuperator model and the thermodynamic station designation in GasTurb 11 [23].

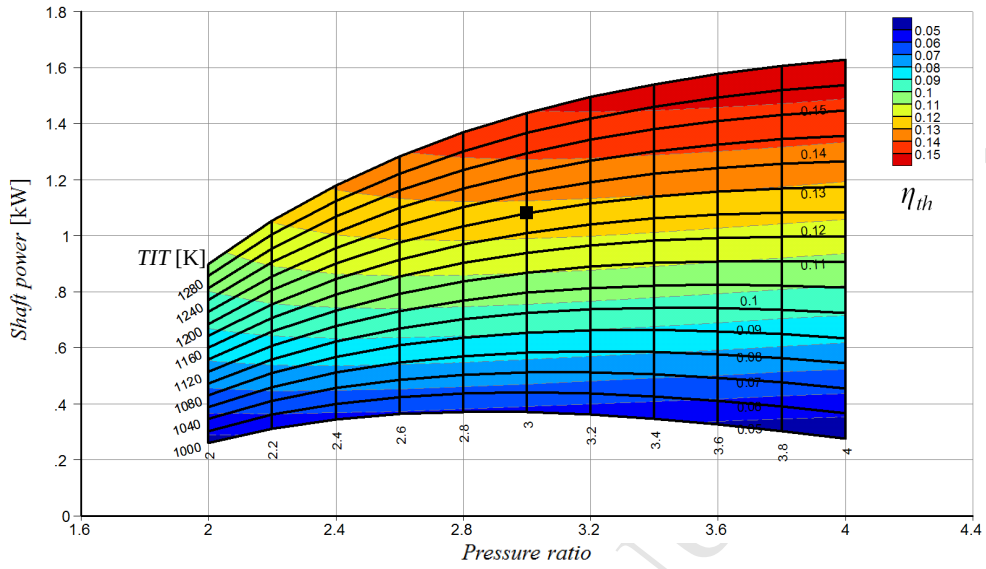

Fig. 2. Parametric study of shaft power and thermal efficiency with change in pressure ratio and TIT of 500-W UMGT power generator.

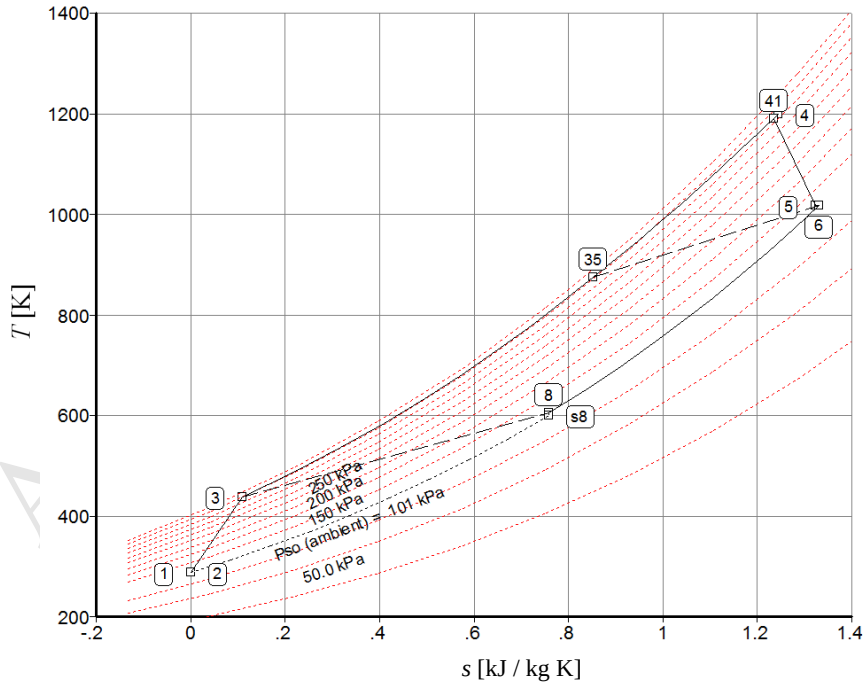

Fig. 3. Temperature-entropy diagram of 500-W UMGT power generator.

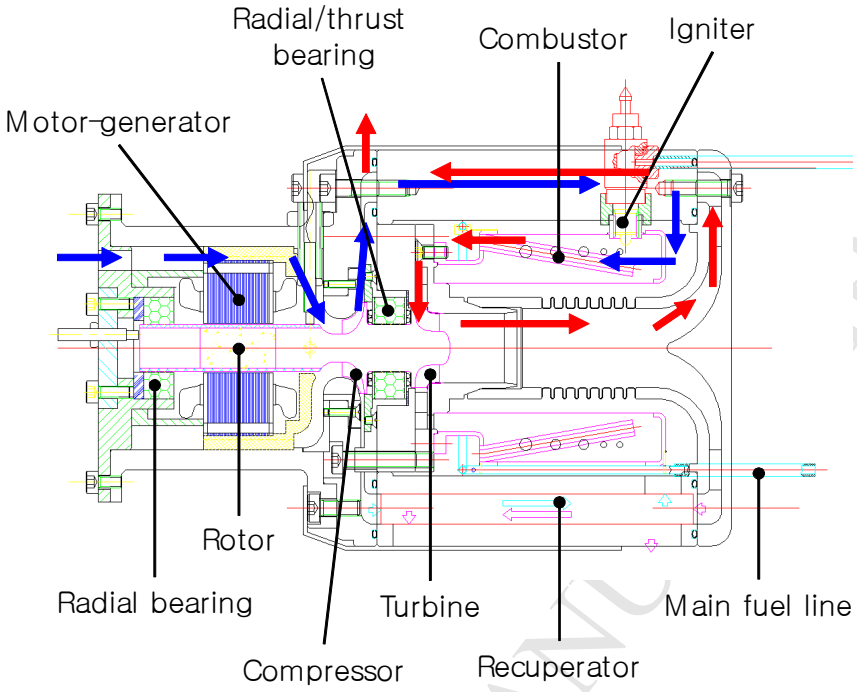

Fig. 4. Schematic cross section of the UMGT power generator [22].

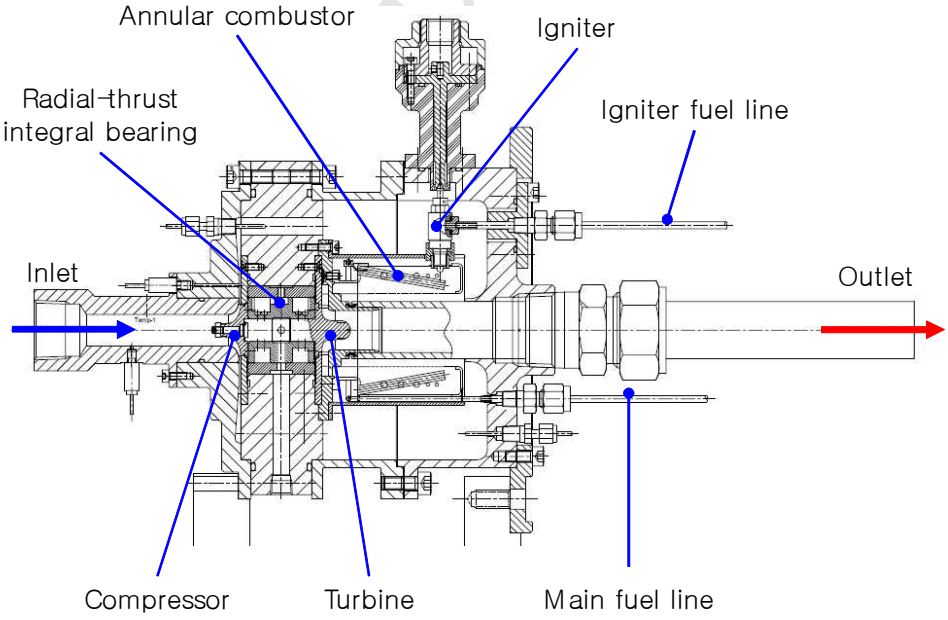

Fig. 5. Schematic layout of the first integrated test rig [22].

(a)

(b)

(c)

(d)

(e)

(f)

Fig. 6. Elements of the first integrated test rig: (a) compressor, (b) turbine, (c) rotor shaft with compressor and turbine, (d) radial-thrust integral static air bearing, (e) graphite hot-bulb igniter, and (f) annular-type combustor with 12 nozzles.

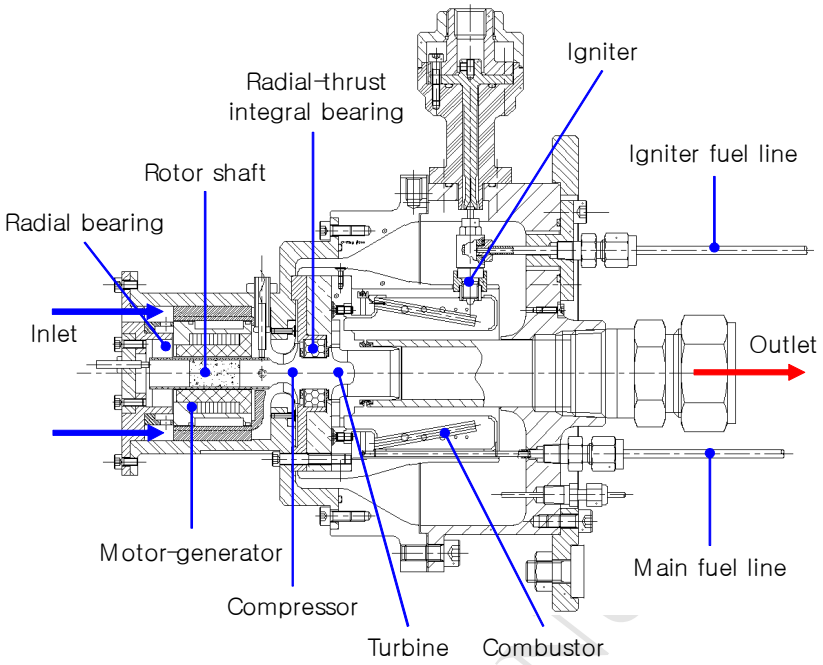

Fig. 7. Schematic layout of the second integrated test rig.

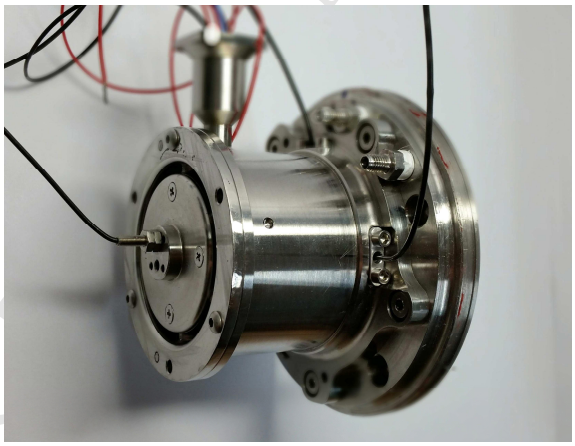

(a)

(b)

(c)

Fig. 8. Elements of the second integrated test rig: (a) motor-generator, (b) rotor shaft with compressor and turbine, and (c) radial-thrust integral MMBFB.

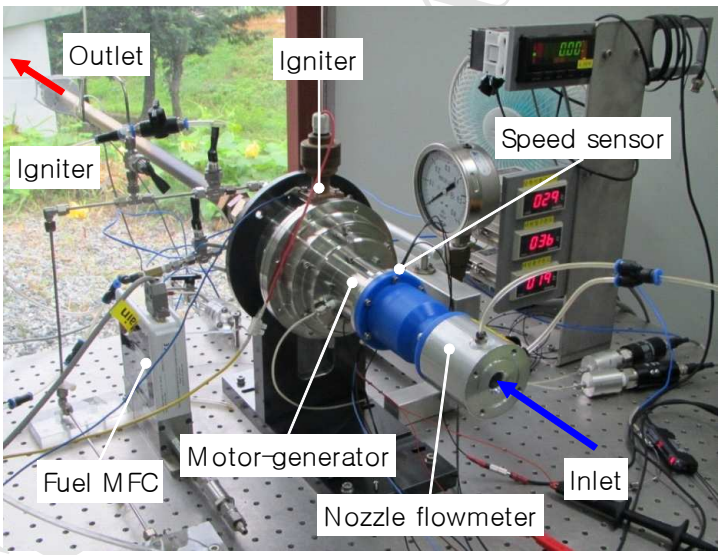

Fig. 9. Test bench for the second integrated test rig.

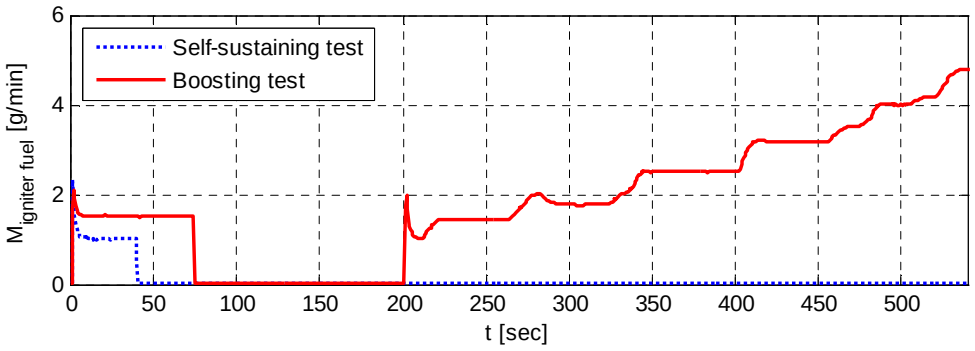
Self-sustaining test
Boosting test
$M_{igniter\ fuel}$ [g/min]
t [sec]
0
2
4
6
0
50
100
150
200
250
300
350
400
450
500

(a)

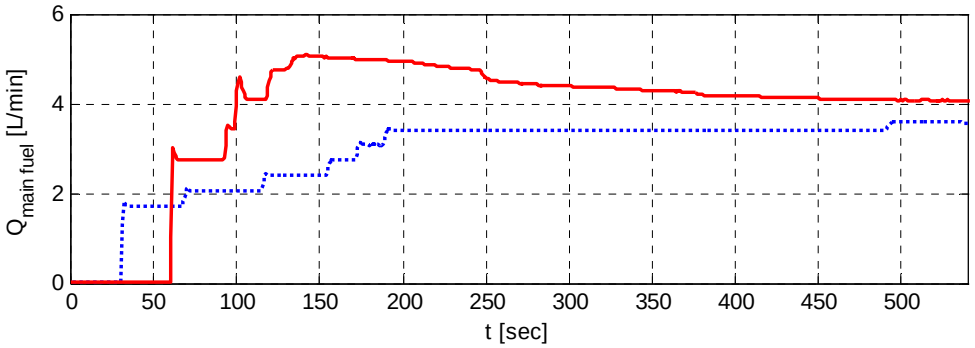
$Q_{main\ fuel}$ [L/min]
t [sec]
0
2
4
6
0
50
100
150
200
250
300
350
400
450
500

(b)

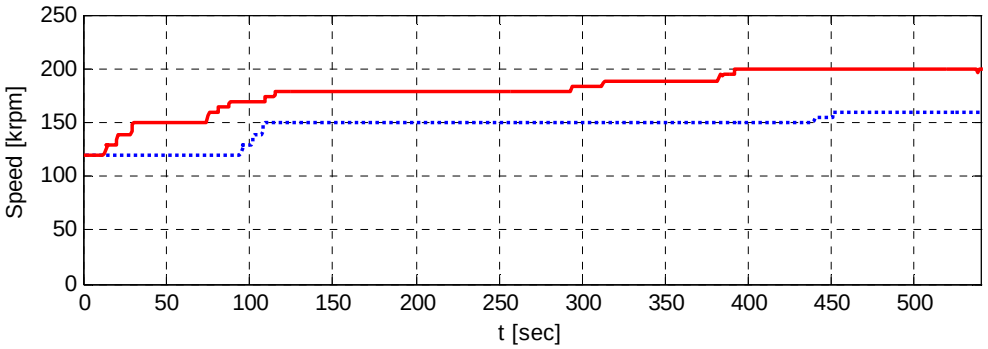
Speed [krpm]
t [sec]
0
50
100
150
200
250
0
50
100
150
200
250
300
350
400
450
500

(c)

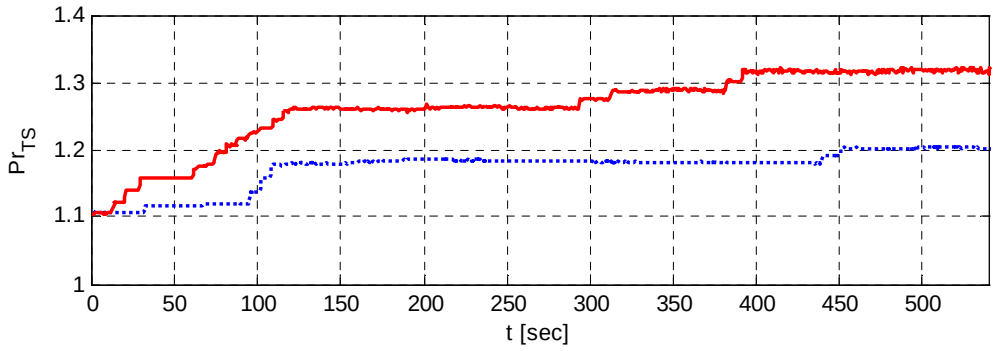
1.4
1.3
1.2
1.1
1
Pr_{TS}
0
50
100
150
200
250
300
350
400
450
500
t [sec]

(d)

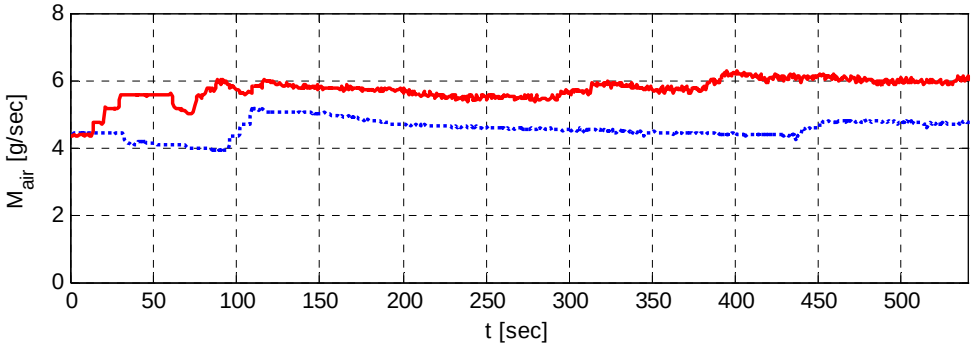
8
6
4
2
0
M_{air} [g/sec]
0
50
100
150
200
250
300
350
400
450
500
t [sec]

(e)

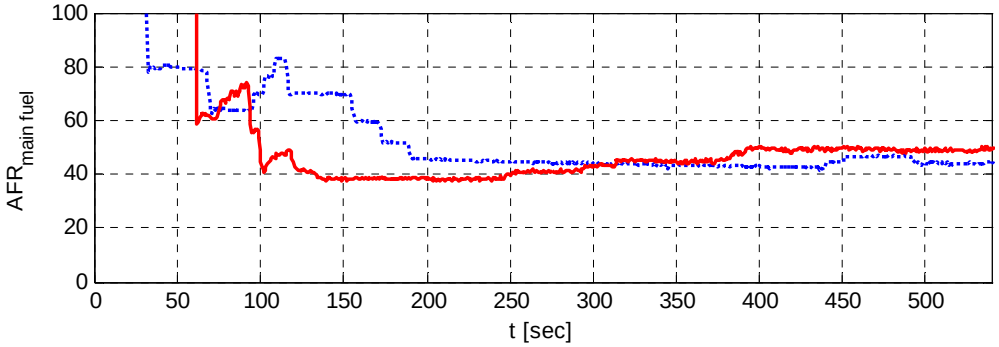
100
80
60
40
20
0
$AFR_{main\ fuel}$
0
50
100
150
200
250
300
350
400
450
500
t [sec]

(f)

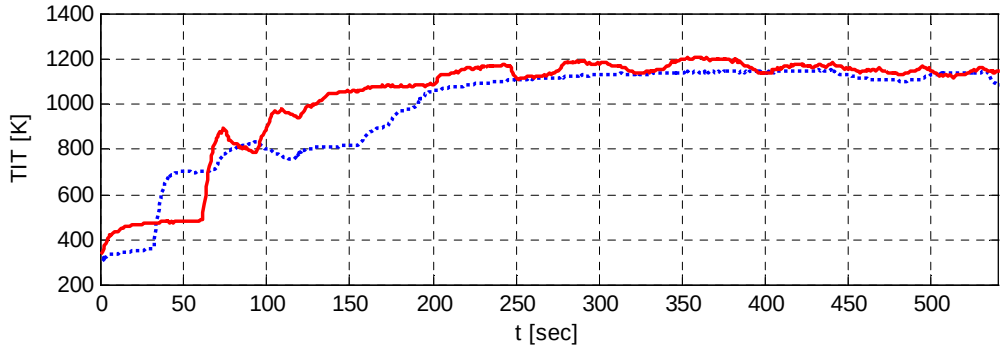

(g)

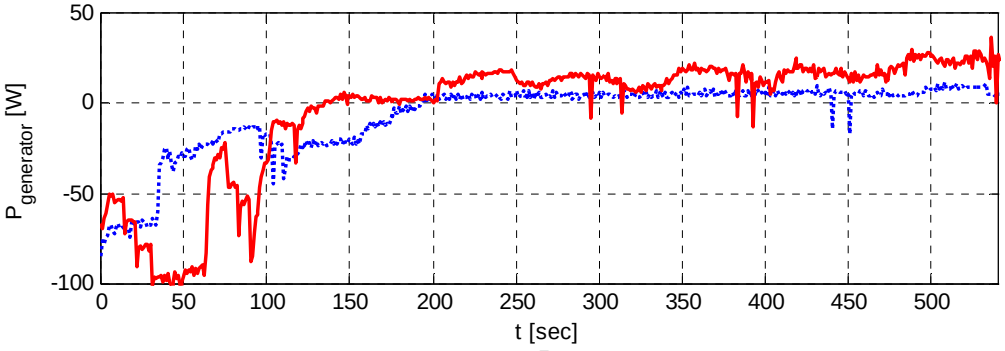

(h)

Fig. 10. Results of electric-power generation test: (a) mass flow rate of igniter fuel, (b) volume flow rate of main fuel, (c) rotational speed, (d) total-to-static pressure ratio of compressor, (e) air mass flow rate, (f) AFR of main fuel, (g) turbine inlet temperature, and (h) generator power.

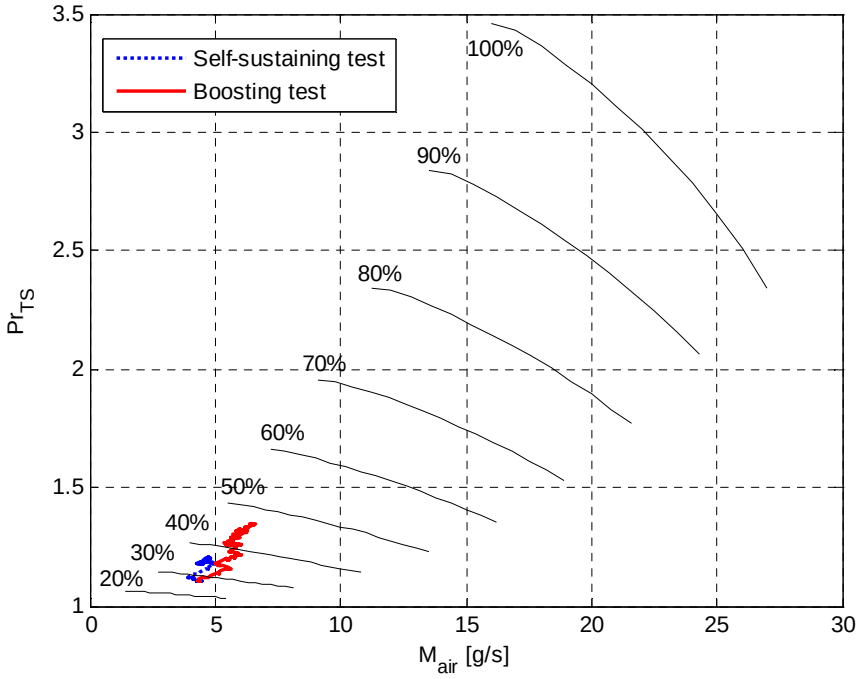

Fig. 11. Compressor performance map for total-to-static pressure ratio.

- We developed integrated test equipment for a 500-W ultra-micro gas turbine power generator.
- The tests were conducted in self-sustaining and boosting modes.
- In the self-sustaining operation, the test rig worked stably and produced 5 W of electric power.
- In the boost operation, the test rig produced 30 W of electric power.
- We verified the feasibility of a 500-W UMGT power generator for electric-power generation.